RSC Advances

L-Phenylalanine methyl ester hydrochloride as green corrosion inhibitor for mild steel in hydrochloric acid solution and effect of surfactant additive

Journal:	*RSC Advances*
Manuscript ID	RA-ART-11-2015-024630.R1
Article Type:	Paper
Date Submitted by the Author:	16-Dec-2015
Complete List of Authors:	Mobin, Mohammad; Aligarh Muslim University, Applied Chemistry ZEHRA, SAMAN; Aligarh Muslim University, Applied Chemistry ASLAM, RUBY; Aligarh Muslim University, Applied Chemistry
Subject area & keyword:	Materials < Physical

L-Phenylalanine methyl ester hydrochloride as green corrosion inhibitor for mild steel in hydrochloric acid solution and effect of surfactant additive

Mohammad Mobin*, Saman Zehra and Ruby Aslam

Corrosion Research Laboratory, Department of Applied Chemistry, Faculty of Engineering and Technology, Aligarh Muslim University, Aligarh 202002, India

* Tel.: +91 5712703515-3003 (Extn.)

E-mail: drmmobin@hotmail.com

The inhibitive effect of L-Phenylalanine methyl ester hydrochloride (PMEH) on the corrosion of mild steel (MS) in 1M HCl solution was investigated at different concentrations and temperatures (30-60 °C) by using weight loss measurements, potentiodynamic polarization measurement, electrochemical impedance spectroscopy (EIS), UV-visible spectrophotometry, and quantum chemical calculations. The obtained results revealed that PMEH is a good inhibitor for the corrosion of MS in HCl solution. The inhibition efficiency (IE) increased with the inhibitor concentration up to 400 ppm as well as with rise in temperature, which is suggestive of chemical adsorption mechanism. The adsorption of inhibitor onto the MS surface was found to obey the Langmuir adsorption isotherm. Thermodynamics of adsorption such as enthalpy of adsorption (ΔH), entropy of adsorption (ΔS), equilibrium of adsorption (K_{ads}), Gibbs free energy (ΔG□), activation and synergism parameters (S_1) were calculated and discussed. Corrosion attack morphologies as observed by scanning electron microscopy (SEM) and energy dispersive X-ray spectroscopy (EDX) verify qualitatively the results obtained by gravimetric as well as electro-chemical methods. The results obtained from all the techniques are in good agreement.

1. Introduction

Corrosion processes are accountable for numerous losses mainly in the industrial scope. It is a constant and continual problem; often difficult to get rid of it completely, the best way to tackle it is prevention. Mild steel (MS), because of economic considerations and excellent properties such as high structural and mechanical strengths, has found applications in a variety of industries such as petroleum, automotive and power and water generation. However, in contact with aggressive acid solutions it corrodes heavily if used without protection. The two mineral acids, which are frequently used in contact with steel at temperatures up to 60 °C, are HCl and H_2SO_4. The acids are generally used to remove rust and scales from the surfaces of ferrous alloys. Among the various methods to shun or prevent devastation or degradation of metal and alloys surfaces, the use of the corrosion inhibitors is the best known low cost and practical method which have great acceptance in the industries.[1-4] The corrosion inhibitors are the chemical substances which retards the corrosion rate when present in the corrosive system at a suitable concentration.[4] They work at the interface of the corrosive media and the metal surface.[5-8] However, most of the compounds used as inhibitor are expensive synthetic chemicals, very unsafe to both human beings and the environments. Thus, the scientific community began searching for cheap, non-toxic environment friendly inhibitors.[9-12]

The inhibitors prevent corrosion by obstructing the active corrosion sites either by forming a protective layer, getting adsorbed, or by forming an insoluble complex on the metal surface.[13-14] Generally, the molecular structure of these compounds plays a key role in determination of their inhibitive performance. Presence of unique atoms such as N, O and S and presence of π - electrons on the double bond and aromatic ring in these compounds determines both the efficiency and adsorption mechanism as their presence favours the adsorption of the inhibitor.[15-18] The IE should increase in the order O < N < S < P. Basically, the adsorption process is constituted of two dependent steps; molecules of inhibitor are transferred from the bulk aqueous media to the double-layer and then adsorbed onto the corroding surface; resulting in construction of a protective layer. These inhibitors may adsorb on the metal/acid solution interface by the following ways: electrostatic interaction between protonated inhibitors and already adsorbed chloride ions or donor–acceptor interactions

between the π-electrons of aromatic ring and vacant d orbital of surface Fe atoms or by the interaction between unshared electron pairs of hetero-atoms and vacant d orbital of Fe surface atoms.[19-20]

Amino acids were reported as good and safe corrosion inhibitor for many metals in various aggressive media. Amino acids are nontoxic, biodegradable and relatively cheap. They are of particular importance acting as practical green corrosion inhibitors.[8,21-23] However, the use of a single amino acid as corrosion inhibitor generally has the disadvantage of the high amount of inhibitor usage. In this context, the idea of synergistic corrosion inhibition studies is of great importance as it leads to a decrease in the amount of inhibitor usage, and improves the inhibition effect of the inhibitor at low concentration. Several researchers have studied the synergistic effect of halide ions on the IE of amino acids.[24,25] Surfactants, which have the ability of influencing the properties of surfaces and interfaces, have recently been shown to synergistically improve the inhibitory action of some amino acids at the author's laboratory.[26-28] Amino acids were shown to interact with the surfactants to form a complex structure and help to adhere to surface, which offers great promise in corrosion inhibition. The binding of surfactants to amino acids depends upon the structure, molecular weights, interaction times and charge densities.

In continuation of our work involving amino acids and surfactants additives as corrosion inhibitor for MS corrosion in acid medium we are reporting the corrosion inhibition performance of PMEH, a non toxic derivative of amino acid L-phenylaniline, on MS in 1M HCl solution at temperature 30, 40, 50 and 60 °C using weight loss, potentiodynamic polarization, EIS, UV visible spectroscopy, SEM, EDX, quantum chemical analysis and thermodynamic and activation parameters. The chemical structure of PMEH, represented in Fig.1, reveals the presence of hetero atom, N and O, π - electrons of double bond and phenyl ring in its structure and suggests that it can act as good corrosion inhibitor. Further, the influence of small concentration of anionic surfactant sodium dodecyl sulphate (SDS) on corrosion inhibition behaviour of PMEH has also been investigated. The selected surfactant SDS is readily biodegradable and has quite low toxicity [LD_{50} value of 1288 mg/kg (Rat)] and is of no concern with respect to human health. Further, to ensure that non toxic nature of PMEH is least compromised the SDS has been added in low concentration.

2. Materials and experimental techniques

2.1. Preparation of metal specimen

The experiments were performed on MS specimens having the chemical composition, as analysed by optical emission spectrometer, (in weight %): 0.1611 C, 0.1815 Mn, 0.0178 P, 0.0351 Cr, 0.0539 Mo, 0.0174 Al, 0.0336 V and the remainder Fe. For gravimetric studies MS coupons of size (2.5 x 2.0 x 0.03 cm) and for electrochemical measurements circular specimens of diameter 1 cm^2 were used. The specimens were machined and abraded with a series of emery papers (grade 320-1200), followed by rinsing with acetone as well as with double distilled water and then dried in warm air.

2.2. Preparation of test solution

The aggressive test solution (1M HCl) was prepared by the dilution of analytical grade 35% HCl with double distilled water. The solution of PMEH was prepared in 1M HCl and the desired concentrations in ppm were obtained by appropriate dilution. Each set of PMEH solutions were also prepared by separately adding 5 ppm of SDS.

2.3. Gravimetric study

After accurate weighing, the freshly prepared MS coupons were suspended in 250 ml beakers containing 200 ml of test solution maintained at 30-60 °C using a thermo-stated water bath. After completion of 6 h of immersion, the coupons were taken out, the corrosion products were removed from the surface, dried and then the specimens were again weighed and the difference in weight was recorded. The weight loss taken was the difference between the weight at a given time and the original weight of the specimen. The specimens were immersed in triplicate and the average corrosion rate was calculated. The uncertainty for triplicate measurements was less than 5%. The corrosion rate was determined using the following equation:

$$\mathrm{R} = \frac{87.6W}{DAT} \qquad (1)$$

where W, is weight loss in mg, D, is the density of specimen in g/cm^3, A, is the area of specimen in cm^2 and T, is exposure time in h. The EI% was calculated by using the following equation:

$$\%IE = \frac{CRo - CRi}{CRo} \times 100 \quad (2)$$

Where, CR_o and CR_i are the corrosion rates of MS in the absence and presence of the inhibitor, respectively. Surface coverage (θ) was evaluated at constant temperature and for different concentrations of inhibitor in 1M HCl from weight loss measurements according to equation:

$$\theta = \frac{CR_0 - CR_i}{CR_0} \quad (3)$$

To judge whether synergism is taking place, the synergism parameter, S_1 was calculated using the following relationship:[29]

$$S_1 = \frac{1 - I_{1+2}}{1 - I'_{1+2}} \quad (4)$$

where, $I_{1+2} = (I_1 + I_2)$; I_1 is IE of PMEH, I_2 is IE of SDS, and I'_{1+2} being IE of PMEH in combination with SDS. S_1 approaches 1 when no interaction between, the inhibitor molecules exists while $S_1>1$ indicates a synergistic effect. In the case of $S_1<1$, antagonistic behaviour prevails which may be attributed to competitive adsorption.

2.4. Potentiodynamic polarization study and AC Impedance

The electrochemical measurements were carried out on Autolab Potentiostat/Galvanostat, model 128N with inbuilt impedance analyzer FRA2. The experiments were carried out using a corrosion cell from Autolab with Ag/AgCl electrode (saturated KCl) as reference electrode, Pt wire as counter electrode and MS specimens with exposed surface area of 1 cm^2 as working electrode. A Luggin-Haber capillary was also included in the cell set up and the tip of the capillary was kept very close to the surface of the working electrode to minimize IR drop. The specimens were allowed to stabilize in the test solution for 30 min prior to the experiments. All the experiments were done at room temperature (30±1°C). Each experiment was repeated at least three times to check the reproducibility of results, and acceptable reproducibility was obtained. The potentiodynamic polarization measurements were performed at a scan rate of 0.001 V/s in the potential range of

0.250 V below the corrosion potential to 0.250 V above the corrosion potential. EIS measurements were implemented at open circuit potential within frequency range of 10^{-2} to 10^{5} Hz with 10 mV perturbation.

2.5. Quantum chemical calculations

Quantum chemical computations were carried out at Restricted Hartree–Fock level (RHF) using PM6 (parametric method 6) semi-empirical methods by MOPAC 9.0 quantum chemical package. The calculated parameters are, the energy of highest occupied molecular orbital (E_{HOMO}), the energy of lowest unoccupied molecular orbital (E_{LUMO}), the separation energy ΔE (E_{LUMO}-E_{HOMO}), the dipole moment (μ), and the fraction of electrons transferred from the inhibitor to iron surface (∆N). Frontier molecular orbitals could be used to speculate the adsorption centres in the inhibitor molecule.

2.6. UV-Vis spectroscopy

UV–visible absorption spectroscopic method was carried out for 1M HCl solution containing 400 ppm of inhibitor before and after 6 h of MS immersion in order to confirm the possibility of the formation of the inhibitor-metal complex. The spectra were obtained using a Perkin–Elmer UV–visible Lambda 25 spectrophotometer and the data was analyzed using the Perkin Elmer UV Winlab Data Processor and viewer.

2.7. SEM-EDX

The surface morphologies of MS surface immersed in the aggressive acid solution in the absence and presence of inhibitor was evaluated using JEOL (Japan) SEM (Model: JSM- 6510LV). After completion of immersion, the test specimens were thoroughly washed with double distilled water, dried with warm air and then subjected to SEM. Compositional analysis of the surface film was carried out by energy dispersive X-ray (EDX) spectroscopy during SEM measurements.

3. Result and discussion

3.1. Gravimetric study

3.1.1. Effect of concentration and temperature. The corrosion inhibition of MS in 1M HCl in absence and presence of varying concentrations of the PMEH alone (50-1000 ppm) and in combination with 5 ppm of SDS, after 6 h of immersion was studied at different temperatures (30- 60 °C) by using weight loss technique. The values of the corrosion rate and IE are depicted in Table 1. From the Table 1, it is apparent that the corrosion inhibiting tendency of the PMEH increases with increasing concentration up to 400 ppm, as on increasing the concentration of the inhibitor, the number of inhibitor molecules adsorbing on the MS surface increases, which leads to the formation of a protective layer resulting in an increase in the IE.[30] However, the increase in the concentration of inhibitor above 400 ppm results in decrease in the IE due to desorption of the inhibitor molecules from the MS surface. From Table 1 it is also clear that the corrosion rate increases with rise in the temperature at the same inhibitor concentration, as increase in the temperature results in the stepping up of the thermal agitation of the molecule of the medium and increase in the conductivity and hence the corrosive action of the medium. The corrosion IE increases with increasing temperature from 30-60 °C. The inhibitor PMEH is more effective at inhibiting the corrosion of steel at low and relatively high temperatures. An increase in IE with rise in temperature at all the concentrations suggests chemical adsorption, which is due to the interaction between the de-localized electrons of the -NH_2 and the vacant, low-energy *d*-orbitals of Fe surface atoms. Further, at high temperatures desorption of water molecules from the steel surface is more favoured leaving larger steel surface area available for the adsorption of the PMEH molecules.

Considering the effect of anionic surfactant, SDS on the corrosion inhibition behavior of PMEH, the addition of SDS causes an increase in the IE of PMEH at all concentrations, which can be explained in terms of the interaction between the PMEH and SDS molecules leading to the improved adsorption on the MS surface. The anionic SDS may bind with protonated PMEH and help to adsorb at the steel surface more firmly and display higher IE. The values of synergism parameter for the

various concentrations of PMEH in combination with fixed concentration of SDS were calculated from the gravimetric data at 30-60 °C and the results are given in Table 1. The values are all greater than unity. This is an indication that the enhanced IE is synergistic in nature and proves that addition of a very small concentration of SDS can significantly improve the adsorption of PMEH on the MS surface.

3.1.2 Effect of immersion time. The effect of immersion time on the IE of PMEH for MS corrosion in 1M HCl, was studied by immersing the steel specimen in 400 ppm inhibited acid solution for exposure period extending up to 160 h at 30 °C and the results are produced in Fig. 2. There is a rapid increase in the IE with increasing immersion period up to 8 h; this is followed by slow increase in IE with further increase in immersion period up to 48 h. After time period extending 48 h there is a decrease in IE, which finally became almost constant after 96 h. The increase in the IE with increasing immersion time is attributed to an increase in the number of PMEH molecules adsorbing on the MS surface, which lead to the formation of a more protective film resulting in an increase in the IE. However, when more inhibitor molecules are adsorbed on the steel surface, the adsorption density of inhibitor becomes sufficiently high and the interactions between inhibitor molecules occur through Van der Waals force. As a result some inhibitor molecules are expected to leave the surface causing a decrease in the effective area covered by the inhibitor and thus causing a decrease in IE. A reasonably high IE exhibited over a long exposure period confirms the stability of adsorbed inhibitor film in 1M HCl solution.

3.1.3. Adsorption isotherm. The adsorption isotherm experiments were accomplished to have more insights into the mechanism of corrosion inhibition, since it provide information about the interaction among the adsorbed molecules themselves and also their interactions with the electrode surface. At different temperatures, the degree of surface coverage (θ) was evaluated from the weight loss measurements and the values were made to fit in various adsorption isotherm models including Langmuir, Temkin, Frieundlich and Frumkin isotherm but by far the results were best fitted in the case of Langmuir adsorption isotherm equation which can be represented by the following equation:

$$\frac{C}{\theta} = \frac{1}{K_{ads}} + C \quad (5)$$

where, K_{ads} is the equilibrium constant of the adsorption process, θ is the degree of surface coverage and C is the inhibitor's concentration (ppm). For the investigated inhibitor at different temperatures, the Langmuir adsorption isotherm is represented in Fig. 3 with slopes close to unity and regression coefficient (R^2) of 0.99 (Table 2). The deviation of slope from unity is due to the interaction among the adsorbed species on the MS. From the intercept of the straight lines, K_{ads} values were obtained and listed in Table 2. The high values for K_{ads} are indicative for a strong adsorption of the inhibitor on MS surface. It is observed that the value of K_{ads} increases with an increase in the temperature suggesting that the strength of adsorption increases with increase in temperature and the adsorbed species could not be easily removed by the solvent molecule from the surface. The free energy of adsorption ($\Delta G°_{ads}$) of the inhibitor on MS surface can be determined using the following equation:

$$K_{ads} = (1/55.5) \exp(-\Delta G_{ads} / RT) \quad (6)$$

where, the value of 55.5 is the concentration of water in the solution expressed in mol L^{-1}, R is the universal gas constant and T is the absolute temperature (K). The calculated values of ΔG_{ads} are shown in Table 2. The larger and negative value of ΔG_{ads} suggests that adsorption of the inhibitor molecule on MS surface in 1M HCl is a spontaneous process and inhibitor is strongly adsorbed on MS surface.[31] Generally, a value of ΔG_{ads} less than −20 kJ/mol is associated with electrostatic interaction between the charged molecules and the charged metal (physical adsorption) while those more negative than −40 kJ mol^{-1} involve sharing or transfer of electrons from the inhibitor molecules to the metal surface to form a co-ordinate type of bond (chemisorption).[32-34] In the present investigation, the values of the ΔG_{ads} range from -20.623 to -24.859 KJ mol^{-1} suggesting comprehensive mode of adsorption (involving both physical and chemical adsorption). Chemisorbed molecules are thought to provide more effective protection since they reduces the inherent reactivity of the metal at the sites where they are attached. But it is difficult to distinguish between chemisorption and physisorption only based on the parameter of ΔG_{ads}.[2] In fact; there is no strict boundary line between physisorption and chemisorption. In addition, it is generally accepted that physical adsorption is preceding stage of chemisorption of inhibitors on the metal surface. [35,36]

3.1.4 Thermodynamic and kinetic parameters. Thermodynamic parameters of adsorption play an important role in understanding the mechanism of adsorption process of the inhibitor molecules on the metal surface. The value of apparent activation energy was calculated by using the Arrhenius rate equation:[37]

$$\mathrm{Log\,CR} = -\frac{E_a}{2.303RT} + logA \qquad (7)$$

where, CR is the corrosion rate, E_a is the apparent effective activation energy, R molar gas constant, T absolute temperature, and A is the Arrhenius constant. Plot of log CR versus 1/T gave straight line with regression coefficient close to unity as shown in Fig. 4. The slope of individual line was determined and the activation energy was calculated using the expression E_a = - (slope) X 2.303R. The calculated values of E_a are summarized in Table 3. The value of E_a for uninhibited acid is higher as compared to inhibited acid system. The lower values of E_a in presence of additives compared to the blank support chemical adsorption mechanism, which suggest that there is appreciable increase in adsorption of inhibitor on MS surface with increase in the temperature. A further decrease in values of E_a in presence of SDS suggests that the process of adsorption is further strengthened in presence of SDS.

To further elucidate the details of the interaction of the inhibitor with MS surface the kinetic-thermodynamic model was employed. Experimental corrosion rate values evaluated from the weight loss data for MS in 1M HCl in the absence and presence of PMEH and PMEH-SDS were used to determine the enthalpy of activation (ΔH) and apparent entropy of activation (ΔS) for the formation of the activation complex in the transition state equation. The transition state equation can be expressed as follows:

$$\mathrm{CR} = \frac{\mathrm{RT}}{\mathrm{Nh}} \exp\left(\frac{\Delta \mathrm{S}}{\mathrm{R}}\right) \exp\left(-\frac{\Delta \mathrm{H}}{\mathrm{RT}}\right) \qquad (8)$$

where, CR is the corrosion rate, N is the Avogadro number, h is the Planck's constant, and R is the molar gas constant. The plots of log (CR/T) against 1/T were drawn and shown in Fig. 5. From the slope (-ΔH/2.303R), and intercept [log(R/Nh) + (ΔS/2.303 R)] of the plots the values of ΔH and ΔS were calculated. The values are listed in Table 3. The positive sign of the ΔH in the absence and presence of inhibitor alone and in combination with SDS reflect the endothermic nature of the MS

dissolution process, which means that the dissolution of MS is difficult in presence of the inhibitors,[38-40] which further confirms that inhibition improves with the temperature. Change in the values of ΔS in the absence and presence of the inhibitor alone and in combination with SDS are negative, implying that formation of activated complex in rate determining step involves association instead of dissociation that is more ordering took place while going from reactants to activated complex.

3.2. Electrochemical measurements

3.2.1. Potentiodynamic polarization study. Potentiodynamic polarization measurements were carried out to distinguish the effect of investigated inhibitor on the anodic dissolution of MS and cathodic hydrogen ion reduction. Typical potentiodynamic polarization curves for MS in 1M HCl in the absence and presence of varying concentration of PMEH alone and in combination with 5 ppm of SDS are shown in Fig. 6. The electrochemical kinetic parameters, e.g., corrosion potential (E_{corr}), corrosion current density (i_{corr}), cathodic and anodic Tafel slopes (b_a and b_c, respectively) derived from the extrapolation of the linear sections of anodic and cathodic branches of polarization curves are depicted in Table 4. It is clearly seen from the Fig. 6 that the nature of polarization curves remains unchanged without and with the inhibitors. The presence of inhibitors only decreases the i_{corr} but does not change the other aspects of the polarization behaviour. The addition of PMEH alone and in presence of SDS causes a shift in the values of E_{corr} slightly toward anodic value (more positive) compared to the blank but no definite shift in E_{corr} is detected. The magnitude of change in the E_{corr} values (less than 85 mV) indicate that PMEH separately and in combination with SDS acts as mixed type inhibitor[39] with predominantly anodic effect, i.e., anodic dissolution of steel is more favored than the cathodic evolution of hydrogen gas. The value of i_{corr} decreased progressively with increasing PMEH concentration, which is further decreased in presence of PMEH + SDS mixture. A decrease in i_{corr} suggest that in presence of inhibitors the rate of electrochemical reaction is retarded due to the formation of protective film on the MS surface, which created a barrier between metal and corrosive acidic medium. The cathodic and anodic Tafel slope values are approximately equivalent with and

without inhibitors suggesting that inhibitors adsorb on MS surface by just blocking the active sites and the processes of anodic and cathodic reactions are unaltered.

The EI% was calculated from i_{corr} using the following equation:[42,44]

$$\%IE = \left(\frac{i^{\circ}_{corr} - i_{corr}}{i^{\circ}_{corr}} \right) \times 100 \quad (9)$$

where, i_{corr}° and i_{corr} are the corrosion current density in absence and presence of the inhibitor, respectively. The obtained values are also listed in Table 4 and follow the same trend as the % IE obtained from gravimetric method.

3.2.2. AC impedance spectroscopy. To explore the kinetics of the electrochemical processes and the inhibition mode occurring at the MS/electrolytic interface impedance experiments were carried out. Nyquist and Bode plots for MS in 1M HCl solution without and with different concentration of PMEH alone and PMEH in combination with SDS (5 ppm) at 30 °C are shown in Fig. 7 (a and b). The addition of inhibitors to the 1M HCl solution does not change the shapes of the Nyquist plots. The plots show single capacitive loop, which is attributed to the charge transfer of the corrosion process. However, the diameter of the capacitive loop gradually increases with increasing concentrations of the PMEH, indicating the adsorption of inhibitor molecules and exhibiting a barrier effect that would effectively protect the MS from aggressive attack by the solution.[6,44] The addition of SDS further causes an increase in the diameter of the circle. Obtained Nyquist plots appears as non-perfect depressed semi circles for all systems over the frequency range of 10^{-2} to 10^{5} Hz with 10 mV perturbation, which is attributed to frequency dispersion effect due to roughness and inhomogeniety of electrode surface, impurities etc, corresponding to one time constant in Bode plots.[2,6]

The EIS results can be modelled by a simple Randel's equivalent circuit as shown in Fig. 8. Rs and Rct represent the solution resistance between the steel electrode and the reference electrode and the charge-transfer resistance corresponding with the corrosion reaction at metal substrate/solution interface, respectively. The double layer capacitance Cdl is placed in parallel to the charge transfer resistance Rct due to the charge transfer reaction. Consequently, in order to compensate the deviations from ideal dielectric behaviour, constant phase elements (CPE) represented by the terms, Y_0 and n were substituted for the pure capacitive elements. The coefficient n

characterizes heterogeneity or the coarseness of the MS surface that causes uneven current distributions on the electrode surface. Impedance of the CPE is given by:[42,45]

$$Z_{CPE} = Q^{-1}(j\omega)^{-n} \quad (10)$$

where, Q and n represent the magnitude and exponent (phase shift) of the CPE, respectively, ω is the angular frequency in rad s^{-1} [$\omega=2\pi f$, where f is the AC frequency in Hz], and j is the imaginary unit which is equal to $(-1)^{1/2}$. For n=0, Z_{CPE} represents a resistance with $R = Q^{-1}$, for n=1 a capacitance with C=Q, for n=0.5 a Warburg impedance with W=Q, and for n=-1 an inductance with $L=Q^{-1}$. The capacitive behaviours of different corrosion systems, the value of Q is converted to Cdl by using the equation:[46]

$$C_{dl} = Q(\omega_{max})^{n-1} \quad (11)$$

where $\omega_{max} = 2\pi f_m$, f_m is the frequency at a the apex of the capacitive loop or at which the imaginary component of the impedance is maximum.[42] The corresponding electrochemical parameters are shown in Table 5. The chi-square (χ^2) value also indicates about the proximity of the circuit with the original phenomena. Lower the χ^2 value, more approximate is the circuit. The range of χ^2 value shows that the equivalent circuit provided a good fit to the experimental data. The semicircles at high frequencies are associated with the electrical double layer capacitors (Cdl) and the diameters of the high frequency semicircles can be considered as the charge-transfer resistance (Rct). The addition of inhibitor to aggressive solution increased the magnitude of R_{ct} representing an increase in the diameter of the Nyquist semicircle, which is attributed to the formation of the protective film at the MS/electrolytic interface. The corresponding decrease in the Cdl value may be due to a decrease in the dielectric constant and/or to an increase in the double layer thickness, which can be attributed to the adsorption of the inhibitor (having lower dielectric constant as compared to the displaced adsorbed water molecule) onto the MS/electrolyte interface, thereby protecting the metal from corrosion.[7,45]

The IE from the impedance data was estimated by comparing the values of the R_{ct} in the absence ($R°_{ct}$) and presence of the PMEH (R_{ct}) alone or in combination with SDS as follows:[47]

$$\%IE = \left(\frac{R_{ct} - R^{\circ}_{ct}}{R_{ct}} \right) \times 100 \quad (12)$$

The corrosion IE increases on increasing the concentration of the PMEH, which is further increased on addition of the SDS.

Bode plots involve only one phase maximum revealing that, in all cases, the corrosion reaction is under charge transfer control and the corrosion process occurring through one step corresponds to one time constant. It is clear that, maximum phase angles are less than -60° indicating the non-ideal capacitive behaviour at intermediate frequencies used. Also the maximum phase angle increases and shifts to lower frequencies with increasing the inhibitor concentration, and this may be due to an increase in the surface coverage of the electrode surface by absorbed barrier layer of the inhibitor and consequently a decrease in the surface roughness. The phase angle at high frequencies provides a general idea of the anti corrosion performance of the inhibitors. The more negative the phase angle the more capacitive the electrochemical behaviour. In Bode phase plot (phase angle vs. frequency) an increase in the inhibitor concentration in test solutions results in more negative values of phase angle at high frequencies. This is indicative of superior inhibitive behaviour of inhibitor at high concentration. In Bode impedance plot (impedance vs. frequency plots) an increase in inhibitor concentrations resulted in an increase in the values of absolute impedance at low frequencies indicating higher protection in inhibited acid solution.

The electrochemical impedance results (EI%) obtained from EIS is consistent with the results obtained from both gravimetric as well as potentiodynamic polarization measurements.

3.2. Quantum chemical calculation In order to analyse the effect of molecular structure and electronic parameters on performance of the studied inhibitor, quantum chemical calculations were carried, as molecular structure of the inhibitor play a vital role in determining its mode of adsorption on the metal surface.[48,49] The optimized molecular structures, HOMO and LUMO orbitals are given in Fig.8. It has been found that the effectiveness of a corrosion inhibitor can be related to its electronic and spatial molecular structure. The computed quantum chemical parameters which are thought important to directly influence on electronic interaction between iron surface

and inhibitor are represented in Table 6. In simple MO theory the HOMO and the LUMO defining the lowest energy transition are the orbitals that drive the chemical reaction. When a molecule is treated as formed by the combination of two fragments; the fragment that acts as a Lewis base (an electron pair donor) supplies the electrons from its HOMO, and the fragment that acts as a Lewis acid (an electron pair acceptor) accommodates the incoming electrons. In a corrosion system, the inhibitor acts as a Lewis base while the metal acts as a Lewis acid. The adsorption of PMEH on steel surface may be achieved by the interaction between the unshared electron pairs on N and O with d-orbitals of iron atoms. The electron configuration of iron, [Ar] $4s^2 3d^6$, indicates that 3d orbital is not fully filled with electron. This unfilled orbital of iron could bond with the highest occupied molecular orbital (HOMO) while the filled 4s orbital could interact with the lowest unoccupied molecular orbital (LUMO) of the PMEH molecule. From the Fig.8, it is found that the electron density of both HOMO and LUMO are localized principally on the N and O atoms and the phenyl ring indicating good adsorption centres, consolidating the opinion of several researchers that pi-electrons and hetero atoms are responsible for inhibition activity.[47-50] Inhibitor could not only donate the electrons to the unoccupied d orbitals of Fe but can also accept electrons from the S-orbital of Fe by using anti-bonding orbital to form a feedback bond. Lower the LUMO energy (ELUMO) level, the easier is the acceptance of electrons of the d orbital of metallic iron. The gap between HOMO–LUMO energy level of molecules is another important parameter that needs to be considered. The smaller is the value of HOMO–LUMO energy gap, the more efficient is the inhibitor. The dipole moment (μ) is an index that can also be used for the prediction of the extent of a corrosion inhibition process. Low values of the μ will favour the accumulation of inhibitor molecules on the metallic surface. The fraction of electrons transferred (ΔN) was calculated by using the equation:

$$\Delta N = \frac{\chi_{Fe} - \chi_{Inh}}{2(\eta_{Fe} - \eta_{Inh})} \quad (13)$$

where χ_{Fe} and χ_{inh} denote the absolute electronegativity of iron and the inhibitor molecule, respectively; η_{Fe} and η_{inh} denote the absolute hardness of iron and the

inhibitor molecule, respectively. These quantities are related to electron affinity (A) and ionization potential:

$$\chi = \frac{(I + A)}{2} \quad (14)$$

$$\eta = \frac{(I - A)}{2} \quad (15)$$

Values of χ and η were calculated by using the values of I and A obtained from quantum chemical calculation.

$$I = -E_{HOMO} \quad (16)$$

$$A = -E_{LUMO} \quad (18)$$

The theoretical values of χ_{Fe} and η_{Fe} are 7 and 0 eV/mol, for considering metallic bulk, I=A.[51] Values of ΔN exhibit the direction of the electron transfer between inhibitor and metal surface. The value of $\Delta N > 0$ indicates the transfer of the electrons from inhibitor molecule to the metal surface whereas $\Delta N < 0$ indicates transfer of the electrons from the metal surface to the inhibitor molecule. In the present investigation the value of $\Delta N > 0$ indicating electron transfer from PMEH to the steel surface.

3.3. UV-Vis spectroscopy

UV-visible spectroscopy provides substantial support for the formation of complex between the two species in the solution. In order to confirm the formation of the [inhibitor-Fe^{2+}], UV-visible absorption spectra were obtained from 1M HCl solution containing 400 ppm of PMEH before and after 6 h of MS immersion and the same are depicted in Fig 10. The absorption spectrum of solution containing 400 ppm of PMEH before MS immersion (curve a) shows visible absorption band of shorter wave length of 329.17nm. The absorption band may be assigned to π-π* and n- π* transitions involving the whole electronic structure of the inhibitor with a considerable charge transfer character. After 6 h of MS immersion (curve b) there is change in the position of absorption band from 329.17 nm to 338.73 nm (bathochromic shift),

which confirms the formation of complex between PMEH and Fe^{2+} ions released during corrosion reaction of MS in 1M HCl solution.

3.5. SEM-EDX studies

In order to confirm the formation of absorption film surface morphological studies of the MS specimen exposed to uninhibited and inhibited acid solution at 30 °C were carried out by SEM. Fig. 11a shows a freshly polished MS surface, which is free from any noticeable defects except some polishing scratches. SEM image of the MS surface after 6 h of immersion in the uninhibited 1M HCl indicates severely corroded surface morphology characteristics of uniform corrosion due to the corrosive attack of the acid solution (Fig. 10b). Fig. 11 (c and d) present SEM images in the presence of 400 ppm of PMEH alone and in combination with 5 ppm of SDS, respectively. In presence of the PMEH, the surface heterogeneity is markedly decreased and clearly a smooth surface with scattered pits is noticed, which is due to the formation of an inadequate absorption film having some defects. The addition of SDS to the PMEH inhibited acid solution caused additional surface coverage, which lead to formation of a more complete film and as a result further improvement in the surface smoothness was observed.

The EDX spectra of MS in the absence and presence of 400 ppm of PMEH alone and in combination with 5 ppm of SDS in 1M HCl solution are shown in Fig. 12. EDX analysis was done to determine the elements present on the MS surface before and after immersion in uninhibited and inhibited acid solution. EDX spectrum of polished MS before immersion in acid solution shows the characteristics peak of elements constituting the MS (Fig. 12a). EDX spectrum of MS specimen after immersion in 1M HCl solution shows the additional peak of Cl; the peak of O is absent, which is attributed to the breakdown of the oxide film and free corrosion of MS in HCl solution (Fig. 12b). In presence of inhibited acid solutions an additional peak of N is shown, which is attributed to the formation of an absorption film containing N covering the MS surface (Fig. 12 c and d).

4. Conclusion

From the obtained results the following conclusions can be deduced:

1. L-Phenylalanine methyl ester hydrochloride acts as good corrosion inhibitor for mild steel in 1M HCl solution. The inhibition efficiency increases with increase in the inhibitor concentration as well with the rise in temperature from 30-60 °C, which is suggestive of chemical adsorption.
2. The inhibition efficiency of L-Phenylalanine methyl ester hydrochloride is synergistically increased on addition of small amount of SDS (5 ppm) to the aggressive acid solution.
3. The data obtained from weight loss measurements suggest corrosion inhibition by adsorption mechanism and fit well the Langmuir adsorption isotherm at all the concentrations and temperatures studied.
4. Thermodynamic parameters revealed that the adsorption process is spontaneous and comprehensive (involving both physical and chemical adsorption).
5. UV-visible spectroscopic measurements suggest the formation of complex between inhibitor and Fe^{2+} ions released during corrosion reaction.
6. The results of potentiodynamic polarization measurements indicate that inhibitor alone and in combination with SDS acts as mixed type inhibitor. The change in impedance parameters indicated that L-Phenylalanine methyl ester hydrochloride and L-Phenylalanine methyl ester hydrochloride-SDS molecules acted by accumulating at the metal/acid solution interface.
7. The computed values of the quantum chemical parameters support the results of weight loss and electrochemical measurements.
8. The SEM studies showed smoother surface of mild steel in presence of inhibitor alone and in combination with SDS. This further confirms the results of weight loss and electrochemical measurements. EDX results confirmed the formation of an absorption film in presence of inhibitor.

Acknowledgement

One of the authors, Saman Zehra acknowledges UGC-MANF, New Delhi for providing financial assistance.

References

1 M. A. Amin, S. S. Abd El-Rehim, E. E. F. El-Sherbini and R.S. Bayoumi, *Electrochim. Acta*, 2007, **52**, 3588.

2 M. Tourabi, K. Nohair, M. Traisnel, C. Jama and F. Bentiss, *Corros. Sci*., 2013, **75**, 123.

3 R. Yildiz, *Corros. Sci*. 2015, **90**, 544.

4 M. A. Hegazy, A. S. El-Tabei and H. M. Ahmed, *Corros. Sci.,* 2012, **64**, 115.

5 K.C. Emregul and O. Atakol, *Mater. Chem. Phys.,* 2003, **82**, 188.

6 A. Doner and G. Kardas, *Corros. Sci.*, 2011, **53,** 4223.

7 R. Solmaz, G. Kardas, B. Yazıcı and M. Erbil, *Colloid Surf. A*, 2008, **312**, 7.

8 M. Ozcan, F. Karadag and I. Dehri, *Acta Phys. Chim. Sin.,* 2008, **24**, 1387.

9 S. A. Umoren, I. B. Obot and N. O. Obi-Egbedi, *J. Mater. Sci.*, 2009, **44**, 274.

10 O. K. Abiola and A. O. James, *Corros. Sci.*, 2010, **52**, 661.

11 F. S. de Souza and A. Spinelli, *Corros. Sci.,* 2009, **51**, 642.

12 M. S. Morad, *Corros. Sci.*, 2008, **50**, 436.

13 R. Yıldız, T. Dogan and I. Dehri, *Corros. Sci.*, 2014, **85**, 215.

14 R. Solmaz, G. Kardas, B. Yazıcı and M. Erbil, *Colloid Surf.* A, 2008, **312**, 7.

15 D. Daoud, T. Douadi, H. Hamani, S. Chafaa and M. Al-Noaimi, *Corros. Sci.*, 2015, **94**, 21.

16 A. Zarrouk, B. Hammouti, T. Lakhlifi, M. Traisnel, H. Vezin and F. Bentiss, *Corros. Sci.*, 2015, **90**, 572.

17 X. Li, X. Xie, S. Deng and G. Du, *Corros. Sci.*, 2014, **87**, 27.

18 H. Hamani, T. Douadi, M. Al-Noaimi, S. Issaadi, D. Daoud and S. Chafaa, *Corros. Sci.*, 2014, **88**, 234.

19 A. Popova, E. Sokolova, S. Raicheva and M. Christov, *Corros. Sci*., 2003, **45**, 33.

20 A. Kosari, M. Momeni, R. Parvizi, M. Zakeri, M.H. Moayed, A. Davoodi and H. Eshghi, *Corros. Sci.*, 2011, **53**, 3058.

21 A. B. Silva, S. M. L. Agostinho, O. E. Barcia, G. G. O. Cordeiro and E. D. Elia, *Corros. Sci.*, 2006, **48**, 3668.

22 J. J. Fu, S. N. Li, L. H. Cao, Y. Wang, L. H. Yan and L. D. Lu, *J. Mater. Sci.*, 2010, **45**, 979.

23 D. Q. Zhang, Q. R. Cai, L. X. Gao and K. Y. Lee, *Corros. Sci.*, 2008, **12**, 3615.

24 E. E. Oguzie, Y. Li, and F. H. Wang, *J. Colloids Interface Sci.*, 2007, **310**, 90.

25 S. A. Umoren and M. M. Solomon, J. Ind. Engg. Chem, 2015, **21**, 81.

26 M. Mobin and M. Parveen, *J. Disp. Sci. Tech.*, 2014, **35(1)**, 29.

27 M. Mobin, M. Parveen and M.Z.A. Rafiquee, *Arabian Journal of Chemistry*, DOI: 10.1016/j.arabjc.2013.04.006.

28 M. Mobin, M. Parveen and M.Z.A. Rafiquee, *J. Mater. Eng. Perform.*, 2013, **22 (2)**, 548.

29 I.O. Arukalam, *Carbohydr. polym.,* 2014, **112**, 291.

30 V. S. Rao and L. K. Singhal, *J. Mat. Sci.,* 2009, **44***, 2*327.

31 G. Avci, Mater. Chem. Phys., 2008, **112**, 234.

32 W. H. Li, Q. He, S. T. Zhang, C. L. Pei and B. R. Hou, *J. Appl. Electrochem.*, 2008, **38**, 289.

33 R. Solmaz, G. Kardas, B. Yazici and M. Erbil, *Colloids Surf. A*, 2008, **312,** 7.

34 M. Mobin and M. A. Khan, *J. Mater. Eng. Perform.*, 2014, **23,** 222.

35 X. Wang, Y. Wan, Q. Wang and Y. Ma, *Int. J. Electrochem. Sci.,* 2013, **8,** 806.

36 S. Zhang, Z. Tao, S. Liao and F. Wu, *Corros. Sci.*, 2010, **52,** 3126.

37 M. Bouklah, B. Hammouti, M. Lagrenee and F. Bentiss, *Corros. Sci.*, 2006, **48**, 2831.

38 C. M. Goulart, A. Esteves-Souza, C. A. Martinez-Huitle, C. J. F. Rodrigues, M. A. M. Maciel and A. Echevarria, *Corros. Sci.*, 2013, **67**, 281.

39 S. Pournazari, M. H. Moayed and M. Rahimizadeh, *Corros. Sci.*, 2013, **71**, 20.

40 M. Sahin, S. Bilgic and H. Yılmaz, *Appl. Surf. Sci.*, 2002, **195**, 1.

41 H. M. Abd and El-Lateef, *Corros. Sci.*, 2015, **92**, 104.

42 I. Ahamad and M. A. Quraishi, *Corros. Sci.*, 2009, **51**, 2006.

43 S. Zhang, Z. Tao, W. Li and B. Hou, *Appl. Surf. Sci.*, 2009, **255**, 6757.

44 N. Caliskan, E. Akbas, *Mater. Chem. Phys.*, 2011, **126**, 983.

45 M. H. Hussin and M. J. Kassim, *Mater. Chem. Phys.*, 2011, **125**, 461.

46 C. S. Hsu, F. Mansfield, *Corros. Sci.*, 2006, **48**, 3398.

47 D. K. Yadav, B. Maiti and M. A. Quraishi, *Corros. Sci.*, 2010, **52**, 3586.

48 L. Herrag, B. Hammouti, S. Elkadiri, A. Aouniti, C. Jama, H. Vezin and F. Bentiss, *Corros. Sci.*, 2010, **52**, 3042.

49 S. Deng, X. Li and X. Xie, *Corros. Sci.*, 2014, **80**, 276.

50 K. F.Khaled, S. A. Fadl-Allah and B. Hammouti, *Mater. Chem and Phys.*, 2009, **117**, 148.

51 M. J. S. Dewar and W. Thiel, *J. Am. Chem. Soc*., 1977, **99**, 4899.

Table 1 Corrosion parameters for MS in 1M HCl in absence and presence of different concentrations of L-Phenylalanine methyl ester hydrochloride alone and in combination with SDS at 30-60 °C

Inhibitor conc. (ppm)	SDS conc. (ppm)	Corrosion rate (mpy)				Inhibition efficiency (EI%)				Synergism parameter (S_1)			
		30 °C	40 °C	50 °C	60 °C	30 °C	40 °C	50 °C	60 °C	30°C	40 °C	50 °C	60 °C
blank	-	802.794	2174.963	3056.488	7499.897	-	-	-	-	-	-	-	-
50	-	603.264	1592.149	2015.748	4791.053	24.85	26.79	34.05	36.12	-	-	-	-
100	-	524.387	1078.423	1273.719	2665.754	34.68	50.42	58.03	64.46	-	-	-	-
200	-	414.835	916.143	966.9748	2157.435	48.33	57.88	68.36	71.23	-	-	-	-
300	-	384.161	719.096	898.323	1451.923	52.15	66.94	70.61	80.64	-	-	-	-
400	-	299.441	569.668	702.590	855.963	62.7	75.82	77.01	87.59	-	-	-	-
500	-	376.857	704.051	723.040	1155.403	53.06	67.63	76.34	84.59	-	-	-	-
600	-	387.082	728.883	853.041	1186.224	51.783	66.49	72.09	84.18	-	-	-	-
800	-	419.217	768.321	893.941	1380.349	47.78	64.67	70.75	81.59	-	-	-	-
1000	-	423.599	847.198	947.986	1431.473	47.23	61.05	68.98	80.91	-	-	-	-
-	5	624.49	1809.7	2598.0	6657.7	22.21	16.77	15.00	11.23	-	-	-	-
50	5	585.735	1475.294	1957.321	4644.985	27.04	32.17	34.53	38.07	1.77	1.14	1.43	1.25
100	5	457.195	1083.829	1155.403	2227.548	43.09	59.51	60.38	70.29	1.33	1.13	1.22	1.08
200	5	357.868	869.109	835.513	1593.609	55.42	68.09	72.66	78.75	1.28	1.1	1.14	1.05
300	5	265.845	655.848	658.77	1019.56	66.89	76.56	78.45	86.41	1.11	1.1	1.1	1.06
400	5	252.699	483.487	439.959	839.895	68.52	81.13	84.17	88.80	1.24	1.14	1.1	1.12

Table 2 Values of slope, regression coefficient (R), equilibrium constant (K_{ads}) and free energy of adsorption (ΔG_{ads}) at different temperatures

Temp	Slope	R^2	K_{ads}	ΔG_{ads} KJ mol^{-1}
PMEH				
30 °C	1.28	0.99	64.725	-20.623
40 °C	1.08	0.99	84.531	-21.998
50 °C	1.12	0.99	131.03	-23.878
60 °C	0.94	0.98	125.41	-24.496
PMEH + SDS (5 ppm)				
30 °C	1.12	0.99	79.936	-24.069
40 °C	1.05	0.99	94.877	-24.31
50 °C	0.98	0.99	126.98	-24.859
60 °C	0.95	0.99	150.99	-24.572

Table 3 Calculated values of kinetic/thermodynamic parameters for MS in 1M HCl in absence and presence of L-Phenylalanine methyl ester hydrochloride alone and in combination with SDS from weight loss measurements

Inhibitor Conc. (ppm)	SDS Conc. (ppm)	E_a ($KJmol^{-1}$)	ΔH^* ($KJmol^{-1}$)	ΔS^* ($KJmol^{-1}K^{-1}$)
blank	-	58.575	55.948	-4.175
50	-	54.952	51.027	-22.635
100	-	42.162	39.328	-62.793
200	-	38.677	38.964	-65.799
300	-	35.652	32.397	-88.109
400	-	31.325	28.031	-104.463
50	5	53.993	52.348	-18.997
100	5	40.018	39.539	-63.309
200	5	36.916	36.188	-76.351
300	5	33.565	33.048	-88.933
400	5	29.161	28.702	-104.195

Table 4 Potentiodynamic polarization parameters for corrosion of MS in 1M HCl in absence and presence of L-Phenylalanine methyl ester hydrochloride alone and in combination with SDS at 30 °C

Inhibitor Conc. (ppm)	SDS Conc. (ppm)	E_{corr} (mV)	I_{corr} (μA/cm^2)	b_a (mV/dec)	b_c (mV/dec)	Corrosion Rate (mpy)	EI%
Blank	-	-439	520	149	-103	237.503	-
100	-	-426	320	142	-101	146.135	38.47
300	-	-439	230	123	-136	103.622	56.36
400	-	-427	190	125	-92	85.498	63.99
-	5	-435	390	179	-113	181.792	23.46
100	-	-430	260	154	-97	119.579	49.65
300	-	-412	190	288	-102	88.059	62.92
400	-	-414	140	143	-82	64.340	72.91

Table 5 EIS parameters for corrosion of MS in 1M HCl in absence and presence of L-Phenylalanine methyl ester hydrochloride alone and in combination with SDS at 30 ºC

Inhibitor Conc. (ppm)	Surfactant Conc. (ppm)	R_s Ω cm^2	R_{ct} Ω cm^2	Q X10^{-4} ($\Omega^{-1}s^n cm^{-2}$)	n_1	χ^2	C_{dl} μFcm^{-2} X10^{-5}	EI%
Blank	-	2.773	219.54	1.04	0.99	13905	9.99	-
100	-	1.214	369.87	0.969	0.99	22346	9.33	40.64
300	-	1.581	534.87	0.952	0.99	23870	9.17	58.95
400	-	1.017	565.83	0.489	0.99	34139	4.72	61.20
-	5 SDS	20.27	287.34	1	0.99	14037	9.62	23.59
100	5 SDS	0.494	408.23	0.867	0.99	22563	8.35	46.22
300	5 SDS	21.19	552.03	0.845	0.99	3606.3	8.15	60.23
400	5 SDS	9.639	796.69	0.399	0.99	75039	3.88	72.44

Table 6 Calculated quantum chemical data for L-Phenylalanine methyl ester hydrochloride

E_{HOMO} (eV)	E_{LUMO} (eV)	ΔE (eV)	μ	χ	η	ΔN
-9.691	-0.033	9.658	3.367	4.832	4.799	-0.22588

Fig. 1 Structure of L-Phenylalanine methyl ester hydrochloride.

Fig. 2 Effect of immersion time on the inhibition efficiency of L-Phenylalanine methyl ester hydrochloride for MS corrosion in 1M HCl at 30 ºC.

Fig. 3 Langmuir adsorption isotherm plots for (A) L-Phenylalanine methyl ester hydrochloride and (B) L-Phenylalanine methyl ester hydrochloride in combination with 5 ppm of SDS, adsorbed on MS surface in 1M HCl solution.

Fig. 4 Plots of log CR vs 1/T in absence and presence of different concentrations of (A) L- Phenylalanine methyl ester hydrochloride and (B) L-Phenylalanine methyl ester hydrochloride in combination with 5 ppm of SDS.

Fig. 5 Plots of log CR/T vs 1/T plots in absence and presence of different concentrations of (A) L-Phenylalanine methyl ester hydrochloride and (B) L-Phenylalanine methyl ester hydrochloride in combination with 5 ppm of SDS.

Fig. 6 Typical Tafel plots of MS in 1M HCl in the absence and presence of different concentrations of (A) L-Phenylalanine methyl ester hydrochloride and (B) L-Phenylalanine methyl ester hydrochloride in combination with 5 ppm SDS.

Fig. 7 Nyquist and Bode plots for mild steel in 1 M HCl in the absence and presence of different concentrations of (A) L-Phenylalanine methyl ester hydrochloride and (B) L-Phenylalanine methyl ester hydrochloride in combination with 5 ppm SDS.

Fig. 8 The suggested equivalent circuit model for the studied system.

Fig. 9 (A) Optimized molecular structures of L-Phenylalanine methyl ester hydrochloride, (B) HOMO and (C) LUMO orbitals.

Fig. 10 UV–visible spectra of (a) 1M HCl containing 400 ppm L-Phenylalanine methyl ester hydrochloride before MS immersion and (b) 1M HCl containing 400 ppm L-Phenylalanine methyl ester hydrochloride after MS immersion, for 6 h at 30 °C.

Fig. 11 SEM images of MS surface in 1M HCl after 6 h immersion at 30 °C (A) before immersion, (B) after immersion in uninhibited acid, (C) with 400 ppm L-Phenylalanine methyl ester hydrochloride and (D) L-Phenylalanine methyl ester hydrochloride in combination with 5 ppm of SDS.

Fig. 12 EDX spectra of MS specimen in 1 M HCl after 6 h immersion at 30 °C (A) before immersion, (B) after immersion in uninhibited acid, (C) with 400 ppm L-Phenylalanine methyl ester hydrochloride and (D) L-Phenylalanine methyl ester hydrochloride in combination with 5 ppm of SDS.

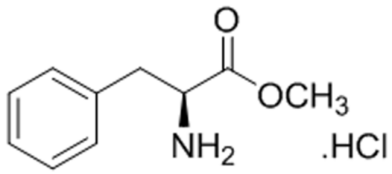

Fig. 1

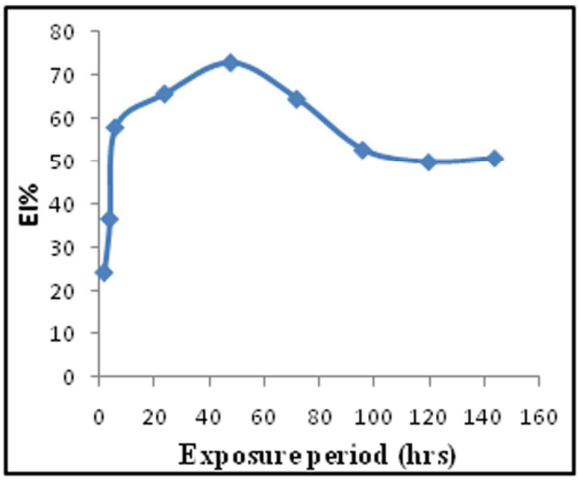

Fig. 2

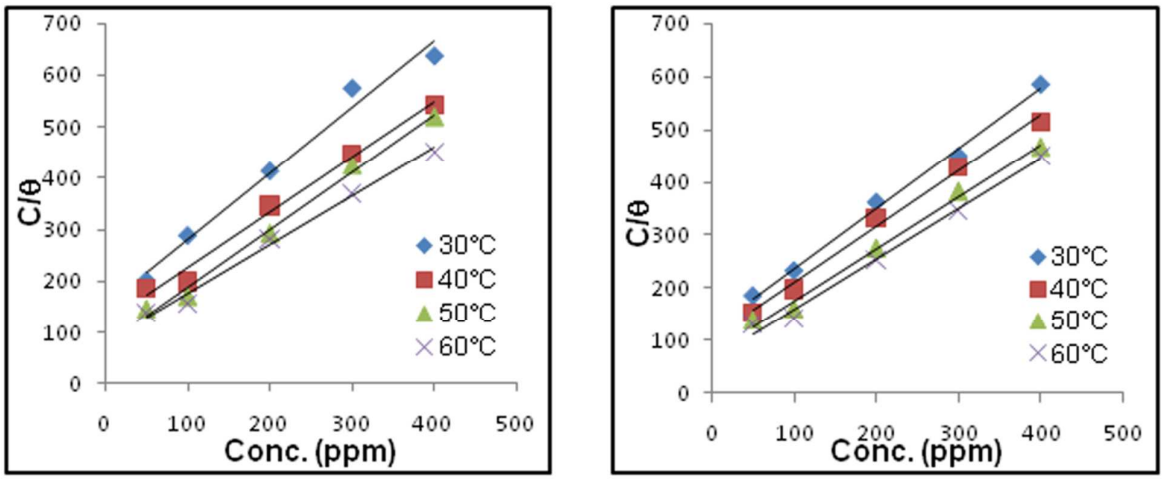

(A) (B)

Fig. 3

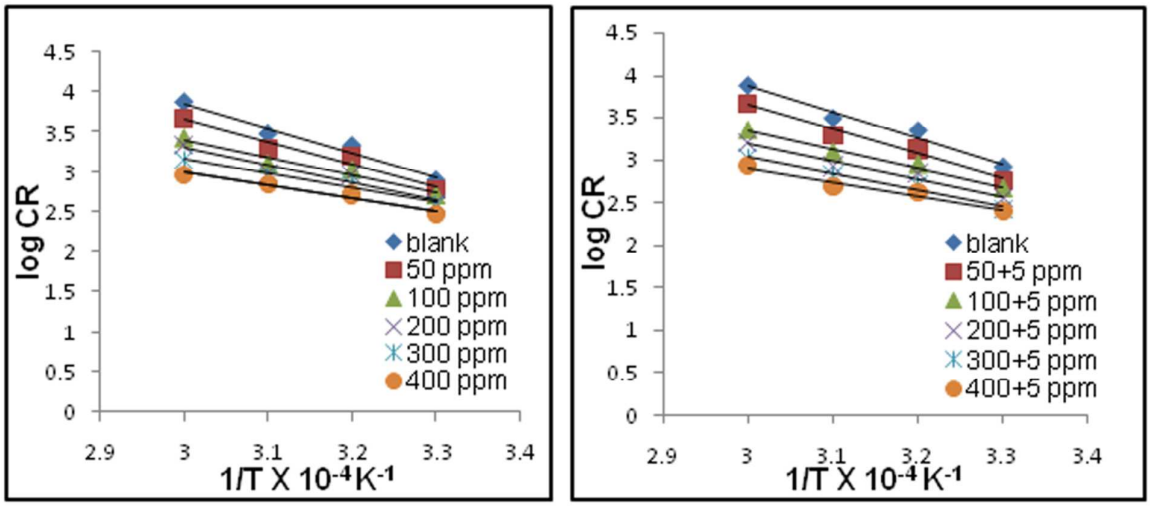

(A) (B)

Fig. 4

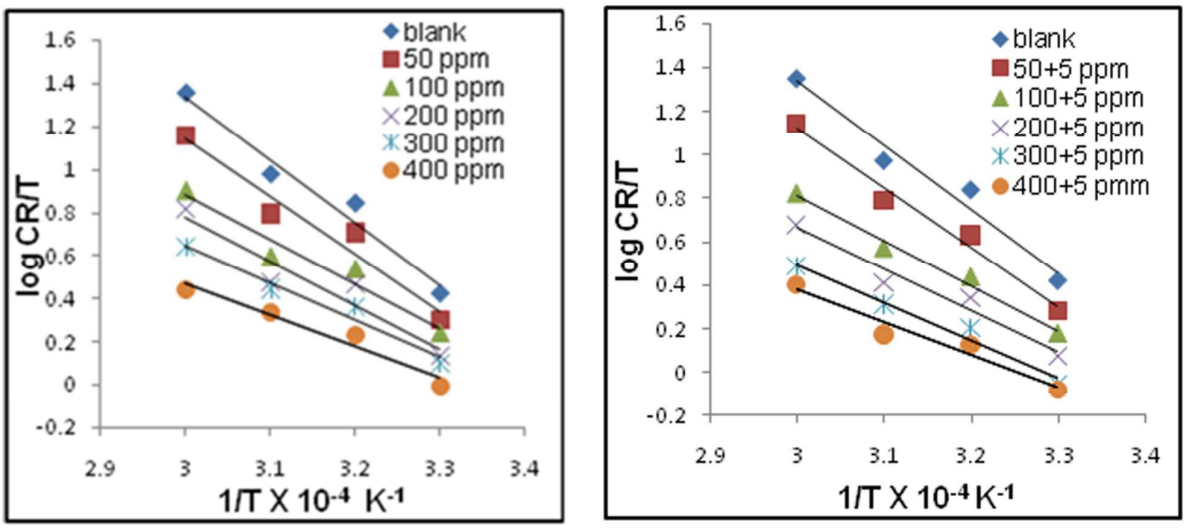

(A) (B)

Fig. 5

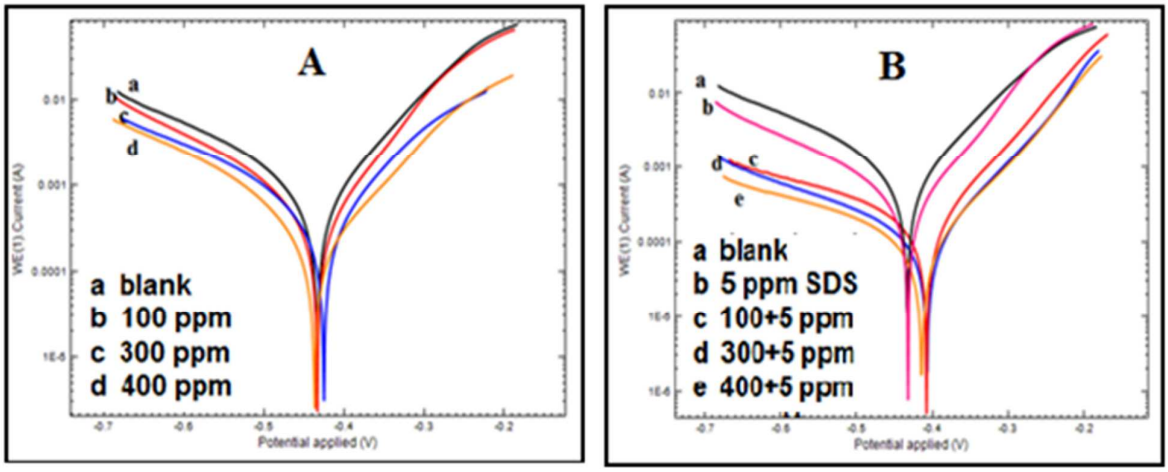
A
a blank
b 100 ppm
c 300 ppm
d 400 ppm
WE(1) Current (A)
Potential applied (V)
B
a blank
b 5 ppm SDS
c 100+5 ppm
d 300+5 ppm
e 400+5 ppm
WE(1) Current (A)
Potential applied (V)

Fig. 6

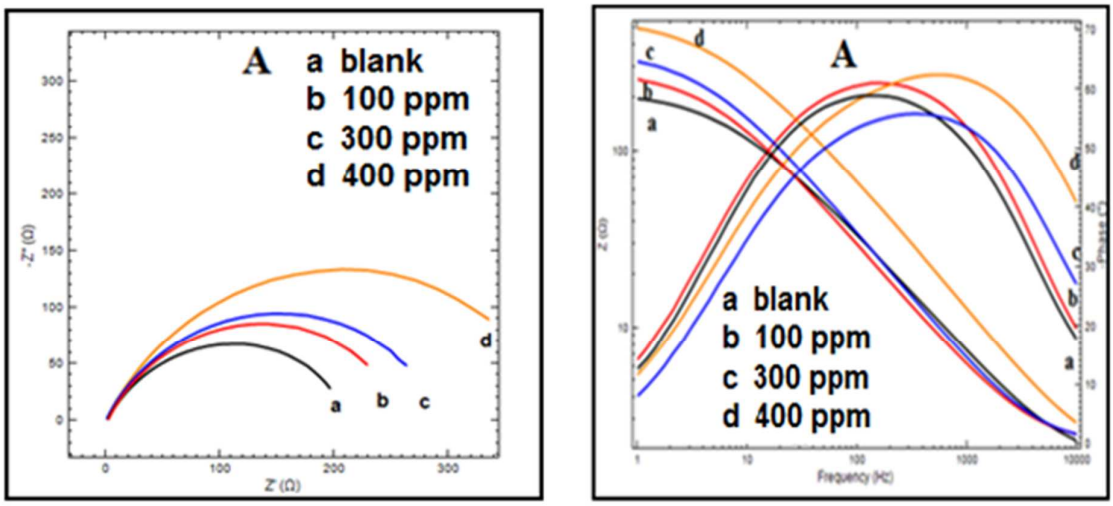
A
a blank
b 100 ppm
c 300 ppm
d 400 ppm
-Z'' (Ω)
Z' (Ω)
A
a blank
b 100 ppm
c 300 ppm
d 400 ppm
Z' (Ω)
Frequency (Hz)

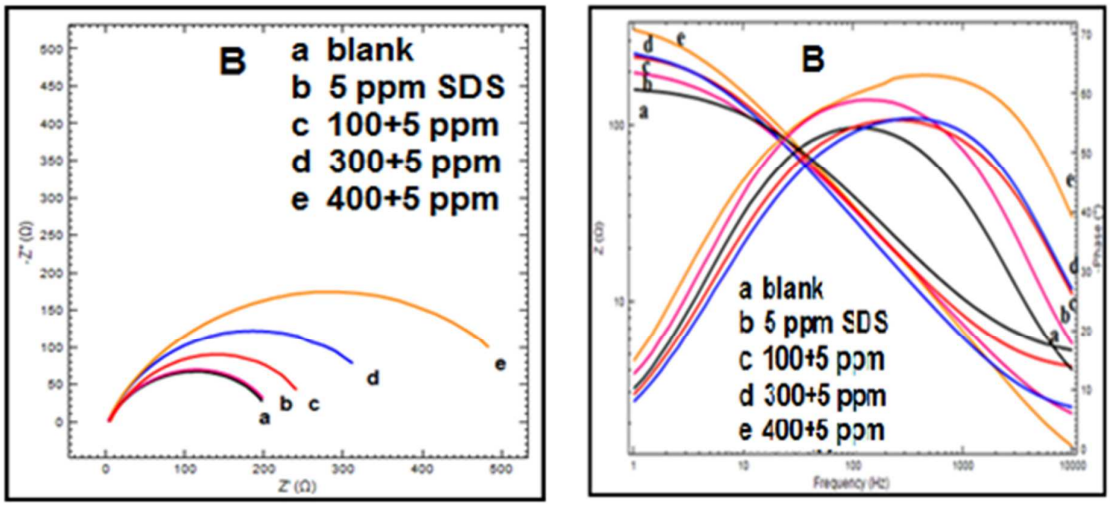
B
a blank
b 5 ppm SDS
c 100+5 ppm
d 300+5 ppm
e 400+5 ppm
-Z'' (Ω)
Z' (Ω)
B
a blank
b 5 ppm SDS
c 100+5 ppm
d 300+5 ppm
e 400+5 ppm
Frequency (Hz)

Fig. 7

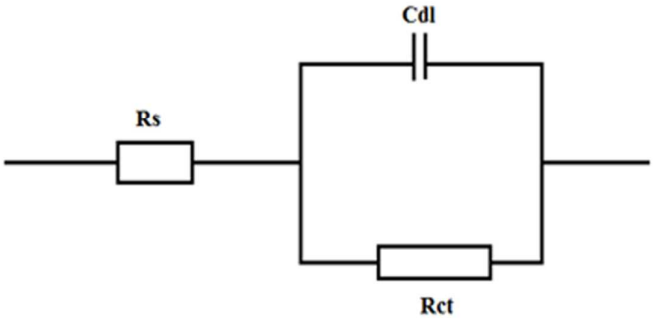
Cdl
Rs
Rct

Fig. 8

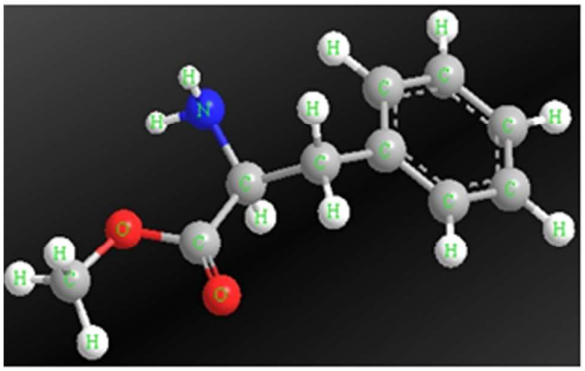

(A)

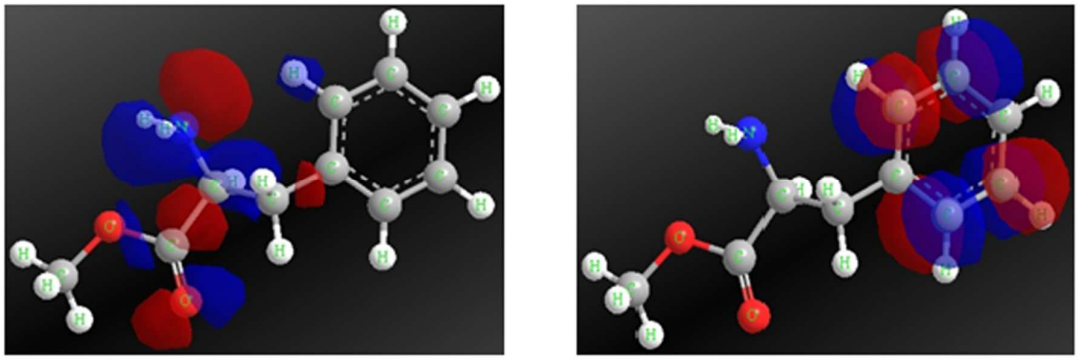

(B) (C)

Fig. 9

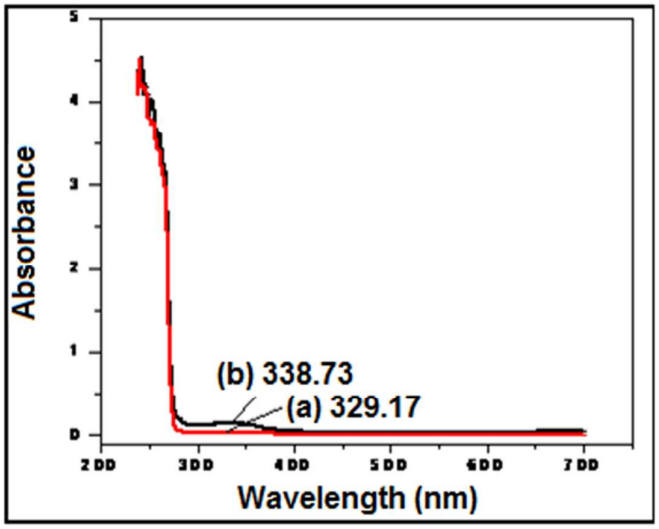

Fig. 10

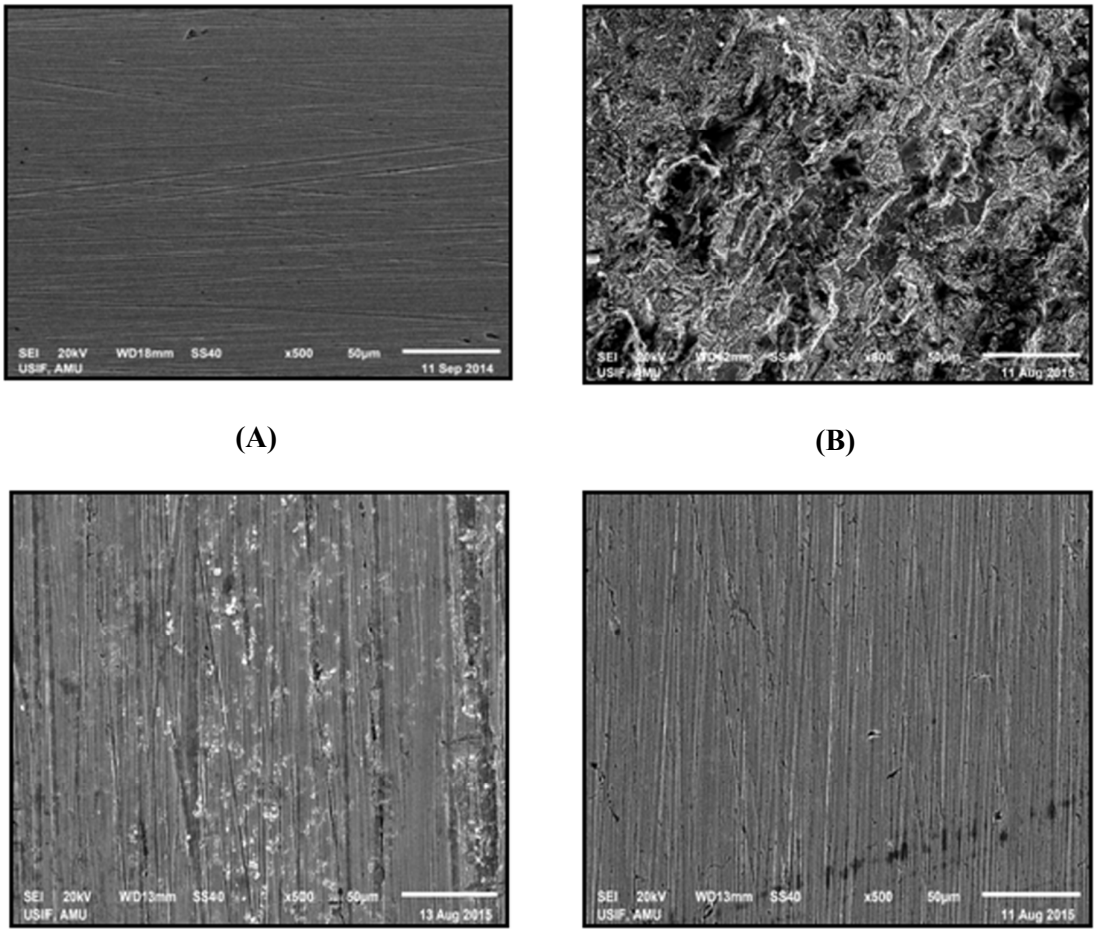
SEI 20kV WD18mm SS40 x500 50µm
USIF, AMU
11 Sep 2014
(A)
(B)
SEI 20kV WD13mm SS40 x500 50µm
USIF, AMU
13 Aug 2015
(C)
SEI 20kV WD13mm SS40 x500 50µm
USIF, AMU
11 Aug 2015
(D)

Fig. 11

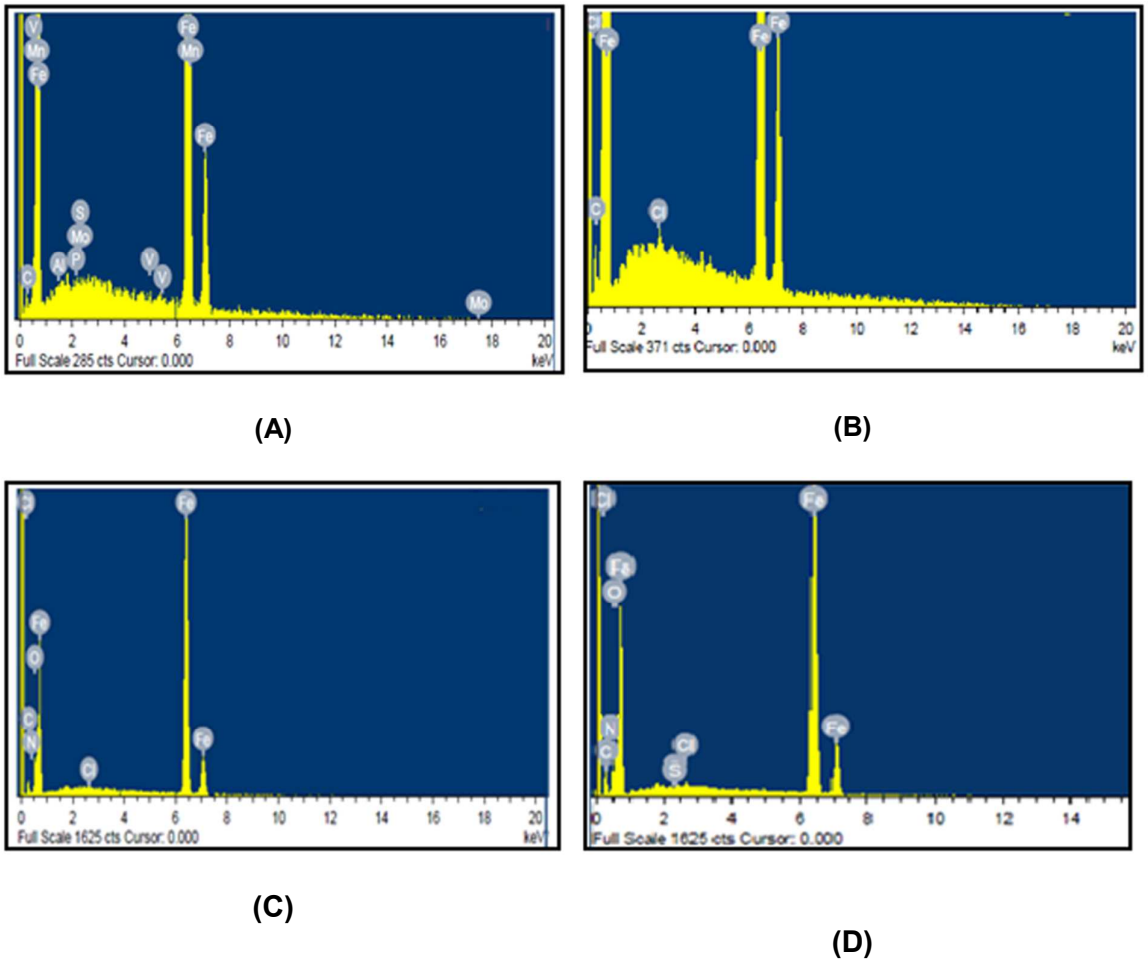
V
Mn
Fe
Fe
Mn
Fe
S
Mo
Al
P
V
V
C
Mo
0 2 4 6 8 10 12 14 16 18 20
Full Scale 285 cts Cursor: 0.000
keV
Cl
Fe
Fe
Fe
C
Cl
0 2 4 6 8 10 12 14 16 18 20
Full Scale 371 cts Cursor: 0.000
keV
Fe
Fe
O
C
N
P
0 2 4 6 8 10 12 14 16 18 20
Full Scale 1625 cts Cursor: 0.000
keV
Cl
Fe
Fe
O
N
C
Cl
S
Fe
0 2 4 6 8 10 12 14
Full Scale 1625 cts Cursor: 0.000

(A) **(B)**

(C) **(D)**

Fig. 12